

# Millimeter-wave detector for gyrotron power monitoring

Cite as: AIP Conference Proceedings **2254**, 090002 (2020); <https://doi.org/10.1063/5.0015430>  
Published Online: 16 September 2020

Weiye Xu, Handong Xu, Fukun Liu, and Xiaojie Wang



View Online



Export Citation

Lock-in Amplifiers  
up to 600 MHz



# Millimeter-wave Detector for Gyrotron Power Monitoring

Weiye Xu<sup>1, a)</sup>, Handong Xu<sup>1, b)</sup>, Fukun Liu<sup>1</sup>, Xiaojie Wang<sup>1</sup>

<sup>1</sup> Institute of Plasma Physics, Chinese Academy of Sciences, Hefei, Anhui, China

<sup>a)</sup>Corresponding author: xuweiye@ipp.cas.cn

<sup>b)</sup>xhd@ipp.cas.cn

**Abstract.** The real-time power monitoring of gyrotron is one of the key issues in the operation of electron cyclotron resonance heating system. The detector can be used for real-time power monitoring. We analyzed the principle of diode detection and designed a D-band wideband detector based on Schottky diode in this paper. The detector includes a waveguide-to-microstrip transition, a matching circuit, a diode, and a low pass filter. A novel waveguide-to-microstrip transition was developed based on probe coupling. A wideband lossy matching circuit was developed based on tapered-line and series matching resistor. The simulation results show that when the input power is -30dBm at 140 GHz, the detection sensitivity is about 1600V/W.

## INTRODUCTION

The RF power measurement of the gyrotron is one of the key issues in the operation of electron cyclotron resonance heating (ECRH) [1] system. There are two methods for measuring gyrotron power, namely the calorimetric method [2] and the detector-based method for real-time power monitoring [3]. Schottky diodes are widely used in millimeter-wave detector designs [4,5], and the cutoff frequency of the diode is now up to THz.

Considering the performance requirements and the processing difficulties of the detector for gyrotron power monitoring in EAST ECRH system, we designed a single diode based D-band (110-170GHz) detector. The detector consists of a waveguide-to-microstrip transition, a matching circuit, a detector diode, and a low-pass filter, which is shown in Fig. 1. The diode is more suitable for transmitting signals using the microstrip line, the microstrip based low pass filter and matching circuit are also easier to implement. However, the waveguide is more suitable for transmitting millimeter waves. It is necessary to couple the microwaves from the waveguide into the microstrip line. A novel waveguide-to-microstrip transition [6] was developed based on probe coupling. In this paper, according to the design process, the detector diode, low-pass filter, and matching circuit are discussed in turn, and then the designed detector is simulated and analyzed.

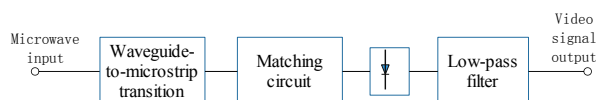


FIGURE 1. Diagram of the detection circuit.

## MILLIMETER WAVE DETECTOR DIODE

The actual ampere-volt (I-V) characteristic of the diode can be divided into three parts: the cut-off area, the working area and the saturation area [7]. The I-V characteristic in the working area is,

$$i(V) = I_s \left( e^{\frac{qV}{nkT}} - 1 \right) \quad (1)$$

Where  $I_s$  is the saturation current of the diode under zero bias. For Schottky diodes,  $I_s$  is generally in the range of  $10^{-14} \sim 10^{-6}$  A;  $q$  is the electron charge;  $V$  is the voltage between the anode and the cathode of the diode;  $k$  is the Boltzmann constant  $1.38 \times 10^{-23}$  J/K;  $T$  is the junction temperature in K;  $n$  is an ideal factor, ideally, its value is 1. Due to the influence of junction defects, etc., the value of  $n$  is greater than 1. The diode can be analyzed with an equivalent circuit, which is shown in Fig. 2. Wherein,  $L_s$  is a series inductance of the pin;  $R_s$  is a series resistance caused by contact, diffusion resistance, etc.;  $R_j$  is a junction resistance, the resistance is related to the bias voltage of the diode;

$C_j$  is a diode junction capacitance, and the capacitance value is related to the bias voltage of the diode;  $C_{pp}$  is a diode shell capacitor (capacitance between two pins). The cutoff frequency of the Schottky diode is,

$$f_c = \frac{1}{2\pi R_s C_j} \quad (2)$$

Generally, the turn-on voltage of a zero-biased Schottky diode (ZBD) is generally less than 100mV. When a ZBD is applied to a detection circuit, it is not necessary to add a bias voltage, which reduces the complexity of the system. We chose to use a G-band (110-300GHz) ZBD produced by VDI. The minimum chip dimensions are 255×88×43 μm (length×width×thickness). The typical forward I-V curve of VDI G-band ZBD is shown in Fig. 4.

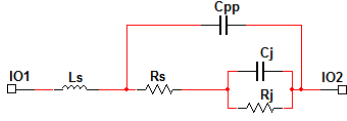


FIGURE 2. The equivalent model of the diode.

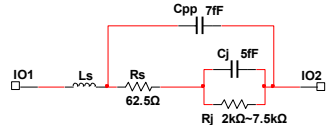


FIGURE 3. Equivalent circuit of VDI G-band ZBD.

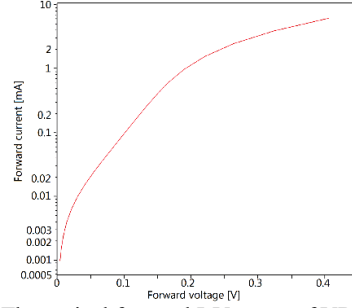


FIGURE 4. The typical forward I-V curve of VDI G-band ZBD.

The equivalent circuit of VDI G-band ZBD is shown in Fig. 3. Where,  $C_j \approx C_T - C_{pp} = 12 \text{ fF} - 7 \text{ fF} = 5 \text{ fF}$ . When the video resistor  $R_v$  is biased at 0V, it can be obtained by dividing the voltage value near 0V by the current value, and its value varies with temperature, which is about 2~7.5 kΩ. We take four points from Fig. 4 ([voltage in mV, current in mA]: [200, 1], [150, 0.5], [70, 0.04], [50, 0.02]) to calculate  $R_s$ ,

$$R_s = \frac{(V_4 - V_3) - (V_2 - V_1)}{(I_4 - I_3) - (I_2 - I_1)} = \frac{(200 - 150) - (70 - 50)}{(1 - 0.5) - (0.04 - 0.02)} \approx 62.5 \Omega \quad (3)$$

So the zero bias junction resistance is,

$$R_j = R_v - R_s \approx R_v \quad (4)$$

Since the junction resistance and saturation current have the following relationship [8],

$$R_j = \frac{dV}{dI} = \frac{V_o}{I_{sat}} \quad (5)$$

Where  $V_o = nkT/q$ , the ideality factor is,

$$n = \frac{q(V_2 - V_1)}{kT \ln(I_2/I_1)} = \frac{q(70 - 50)[\text{mV}]}{kT \ln 2} \approx 1.12 \quad (6)$$

The saturation current is,

$$I_{sat} = \frac{V_o}{R_j} = \frac{nkT}{qR_j} \approx \frac{0.029}{3500} \approx 8.4 \mu\text{A} \quad (7)$$

## LOW-PASS FILTER

When the millimeter wave is input into the detection diode, the DC/low frequency and harmonic signals are generated. What we need is a DC/low-frequency signal proportional to the wave power. The fundamental wave and harmonics need to be suppressed. The low pass filter is used to filter out high-frequency signals.

First, the filter prototype consisting of the inductor and capacitor lumped components was calculated according to the filter design target, and then the inductors and capacitors are converted into microstrip circuits. We want the filter circuit to take up as little space as possible and choose a low-pass filter based on a butterfly radial stub. We designed the filter passband (3dB) with an upper-frequency limit of 50GHz and a 20dB cutoff frequency of 100GHz. The fourth-order maximum flattening filter is used to obtain the lumped parameter filter as shown in Fig. 5.

Then, the lumped elements were converted into microstrip lines. Considering factors such as cost and performance, we chose RT\_Duriod5880 whose dielectric constant is 2.2 as the substrate. The dielectric thickness is designed to be 5 mils, the microstrip line material is copper, and the microstrip line thickness is 0.7 mil. We converted the lumped component capacitance into a butterfly radial stub, and converted the lumped inductors into high impedance lines. The high-impedance line impedance is 100 ohms, the corresponding microstrip line width is 4.494 mils, and the lengths of the two segments are 26.1 mils and 10.8 mils, respectively. As shown in Fig. 6 and Fig. 7, the two butterfly radial stubs have a W of 15.6 mils, an angle of 60°, and a radius R0 of 13.8 mils and 20.7 mils, respectively. The simulation results shown in Fig. 8 show that the insertion loss is 32.8dB and 21dB respectively at 140GHz and 280GHz, and the harmonic signals can be effectively suppressed. In order to further verify the performance of the filter, we

imported the PCB (printed circuit board) layout into the 3D electromagnetic simulation software and simulated it with the finite element method (FEM). The simulation results show that the insertion loss is less than  $-40\text{dB}$  in the  $140\text{GHz}$  and  $280\text{GHz}$  bands.

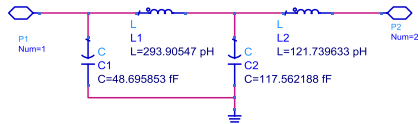


FIGURE 5. Low-pass filter lumped parameter model with a  $20\text{dB}$  cutoff frequency of  $100\text{GHz}$ .

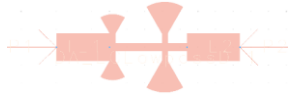


FIGURE 6. The microstrip circuit of the low pass filter.

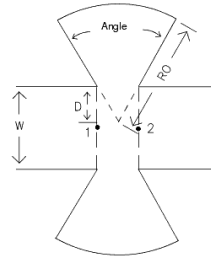


FIGURE 7. The structure of the butterfly radial stub.

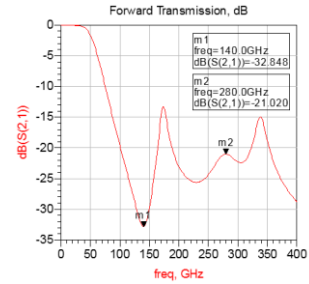


FIGURE 8. The simulation results of the low pass filter.

## MATCHING CIRCUIT

The matching [9] circuit is used to match the input impedance of the detector to a  $50\ \Omega$  impedance to reduce the reflection, so that the microwave power enters the diode as much as possible, improving the detection sensitivity. The matching circuit can easily be designed using the Smith chart. Since the diode IO2 port (shown in Fig. 2) is connected to the low-pass filter, the input impedance of the designed low-pass filter is first analyzed. The simulation results show that the impedance is  $1.56-j*22.5$  at  $140\ \text{GHz}$  (the gyrotron output frequency in the EAST ECRH system is  $140\ \text{GHz}$ ).

The value of  $L_s$  in the diode equivalent circuit shown in Fig. 3 is less than  $0.05\ \text{nH}$ , which can be ignored to analyze the diode input impedance. First, the diode output resistance was set to  $1.56-j*22.5$  (the low-pass filter input impedance at  $140\ \text{GHz}$ ). The parameter sweep of  $R_j$  is performed with a step-size of  $1.5\ \text{k}\Omega$  (from  $2\ \text{k}\Omega$  to  $7.5\ \text{k}\Omega$ ). The simulation results show that the value of  $R_j$  has little effect on the impedance. The impedance varies with frequency, but the change is not very large. At  $140\ \text{GHz}$ , when  $R_j$  is  $3.5\ \text{k}\Omega$ , it is  $14.5-j*119.6$ .

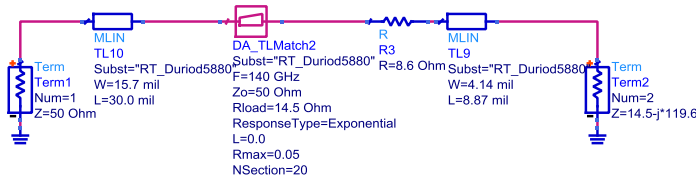


FIGURE 9. Schematic of the impedance matching circuit.

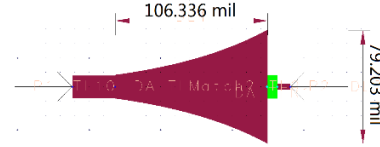


FIGURE 10. Layout of impedance matching circuit.

Since  $R_j$  of the VDI ZBD is about  $3.5\ \text{k}\Omega$  at normal temperature, the input impedance of the diode should be matched to  $14.5-j*119.6\ \Omega$ . The input impedance of the diode varies with frequency. In order to make the diode have the highest sensitivity in the  $110\sim 170\ \text{GHz}$  band, a broadband impedance matching method combining a tapered-line [10] match and a series resistor match was proposed. A resistor is connected in series with the diode input to match the impedance of  $14.5-j*119.6$  to  $14.5\ \Omega$ . The larger the selected resistance value, the wider the available bandwidth, but the lower the sensitivity. We hope that the detection sensitivity is greater than 1000 at  $140\ \text{GHz}$ , and finally,  $R=8.6\ \Omega$  was selected. Then a tapered-line of  $14.5\ \Omega$  to  $50\ \Omega$  is used to obtain the final matching circuit, which is shown in Fig. 9 and Fig. 10. The simulation results show that the VSWR is 1.18 at  $140\ \text{GHz}$ .

We simulated the matching circuit in the  $110\ \text{GHz}\sim 170\ \text{GHz}$  band. The results show that the VSWR in the  $120\ \text{GHz}\sim 170\ \text{GHz}$  band is less than 8.26, and the VSWR in the full range of  $110\ \text{GHz}\sim 170\ \text{GHz}$  is less than 22.52.

## DETECTOR AND THE SIMULATION RESULTS

The detector circuit consisting of a matching circuit, a diode, and a low-pass filter is shown in Fig. 11. The harmonic balance simulation of the detector was carried out. The simulation results (shown in Fig. 12) show that the detector has good linearity for a frequency of  $140\ \text{GHz}$ . When the input power is  $-10\ \text{dBm}$ , the output voltage is about  $0.108\ \text{V}$ , and the detection sensitivity is about  $1080\ \text{V/W}$ . When the input power is  $-20\ \text{dBm}$ , the output voltage is about  $0.015\ \text{V}$ , the detection sensitivity is about  $1500\ \text{V/W}$ ; when the input power is  $-30\ \text{dBm}$ , the output voltage is about  $0.0016\ \text{V}$ , and the detection sensitivity is about  $1600\ \text{V/W}$ . The simulation results when  $L=0$  are similar to the simulation results when  $L=0.05\ \text{nH}$ .

Then the sweep variable was changed from RFPower to Rffreq. The series inductance was set to  $L=0$ . When the input power is set to  $-10\ \text{dBm}$ , the simulation results show that the detection sensitivity is greater than  $500\ \text{V/W}$  in the

frequency range of 123GHz~164GHz, which is shown in Fig. 13. When the input power is set to -20dBm, the simulation results show that the detection sensitivity is greater than 500V/W in the frequency range of 119GHz~166GHz. The series inductance (0 or 0.05nH) has little effect on the results. The sensitivity is close to that of the D-band Zero Bias Detector from Millitech, Inc. or Farran Technology over the entire D-band, and is better at 140GHz. The detector designed in this paper is more suitable for use in the EAST ECRH system.

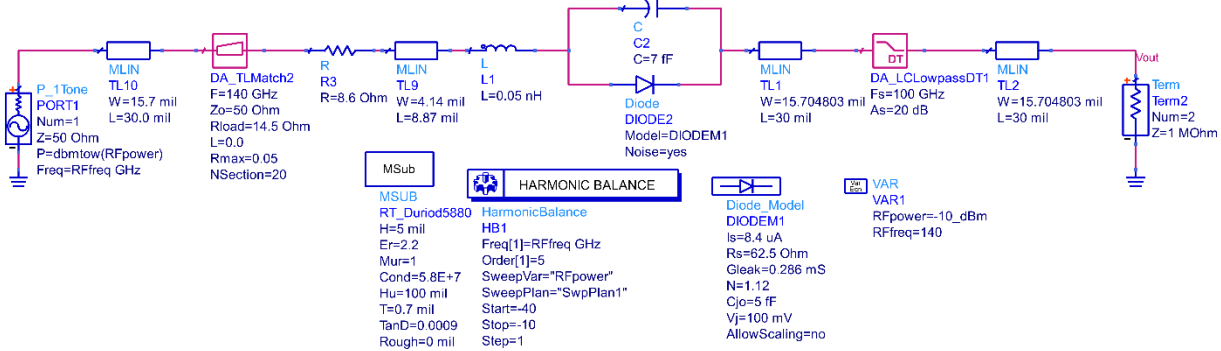


FIGURE 11. The detector circuit and harmonic balance simulation configuration.

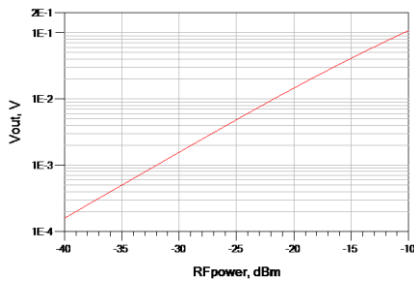


FIGURE 12. Harmonic balance simulation results at 140 GHz.

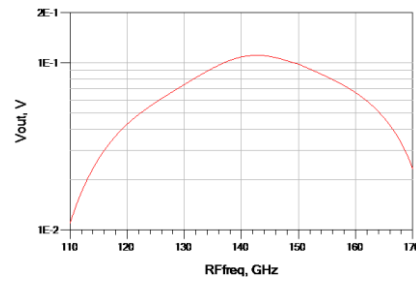


FIGURE 13. Harmonic balance simulation results at -10 dBm.

## SUMMARY

A D-band detector based on Schottky diode was designed in this paper. In order to increase bandwidth, a lossy matching circuit was developed based on tapered-lines and matching resistors. The VSWR is 1.18 at 140 GHz and is less than 8.26 in the 120GHz~170GHz band. The harmonic balance simulation results show that the detection sensitivity is about 1600V/W when the input power is -30dBm at 140 GHz. The processing and testing of the detector will be done in the future.

## ACKNOWLEDGMENTS

This work was supported in part by the National Key R&D Program of China (grant no. 2017YFE0300401) and the National Magnetic Confinement Fusion Science Program of China (grant no. 2015GB102003).

## REFERENCES

1. H. Xu *et al.*, *Plasma Science and Technology* **18**, 442 (2016).
2. W. Xu, H. Xu, F. Liu, J. Wang, X. Wang, and Y. Hou, *Plasma Science and Technology* **19**, 105602 (2017).
3. W. Xu, H. Xu, F. Liu, Y. Tang, Z. Wu, X. Wang, J. Wang, and J. Feng, *IEEE Access* **4**, 5809 (2016).
4. H. Kazemi *et al.*, in *2007 IEEE/MTT-S International Microwave Symposium 2007*, pp. 1367.
5. H. Meinel, *Wissenschaftliche Berichte AEG-Telefunken* **54**, 233 (1981).
6. W. Xu, F. Liu, and H. Xu, *AIP Advances* **6**, 105001 (2016).
7. Weiye Xu. (2017). *Characteristics and Detection Principles of Millimeter Wave Detector Diode (in Chinese)*. [ChinaXiv:201702.00158]. DOI: 10.12074/201702.00158
8. J. L. Hesler and T. W. Crowe, in *Proceedings of the Eighteenth International Symposium on Space Terahertz Technology*, edited by A. Karpov/California Institute of Technology, Pasadena, CA USA, 2007), p. 89.
9. J. Rahola, *IEEE Transactions on Circuits and Systems II: Express Briefs* **55**, 92 (2008).
10. *Microwave Engineering*, 2nd Edition, John Wiley & Sons: New York, 1998, pp. 288-295.